Li et al. Nanoscale Research Letters (2018) 13:120
https://doi.org/10.1186/s11671-018-2540-3

Nanoscale Research Letters

NANO EXPRESS Open Access

Hydrothermal Synthesized of $CoMoO_4$ Microspheres as Excellent Electrode Material for Supercapacitor

Weixia Li, Xianwei Wang*, Yanchun Hu, Lingyun Sun, Chang Gao, Cuicui Zhang, Han Liu and Meng Duan

Abstract

The single-phase $CoMoO_4$ was prepared via a facile hydrothermal method coupled with calcination treatment at 400 °C. The structures, morphologies, and electrochemical properties of samples with different hydrothermal reaction times were investigated. The microsphere structure, which consisted of nanoflakes, was observed in samples. The specific capacitances at 1 A g^{-1} are 151, 182, 243, 384, and 186 F g^{-1} for samples with the hydrothermal times of 1, 4, 8, 12, and 24 h, respectively. In addition, the sample with the hydrothermal time of 12 h shows a good rate capability, and there is 45% retention of initial capacitance when the current density increases from 1 to 8 A g^{-1}. The high retain capacitances of samples show the fine long-cycle stability after 1000 charge-discharge cycles at current density of 8 A g^{-1}. The results indicate that $CoMoO_4$ samples could be a choice of excellent electrode materials for supercapacitor.

Keywords: Hydrothermal method, $CoMoO_4$, Supercapacitor, Electrode material

Background

It is important to develop the conversion and storage of renewable alternative energy because of the rapid decay of fossil fuels. Supercapacitor, as a kind of energy storage device, has attracted much attention in recent years [1–5]. Supercapacitors show desirable performance, such as high power density, short charging time and long cycle life [6–8]. According to the mechanism of charge storage, supercapacitors could be classified into electrochemical double-layer capacitors (EDLCs) and redox electrochemical capacitors (i.e. pseudocapacitance (PCs)). The charge storage mechanism of EDLCs is related to the reversible adsorption and desorption of electrolyte ions on electrode/electrolyte surface, whereas that of PCs is related to the redox reactions on the electrode surface [4, 6, 8, 9]. Therefore, whether for EDLCs or PCs, the electrodes are very important, and it is necessary to find an interesting electrode material for supercapacitor application. Generally, the energy density of PCs is higher than that of EDLCs [10, 11]. Many metal oxide materials, such as NiO [12, 13], Co_3O_4 [3], CuO [14], MnO_2 [15], and SnO_2 [16], have attracted much attention for the use as supercapacitor electrodes. Among these metal oxides, molybdenum oxides and cobalt oxides are the promising candidates for applications due to its high redox activity, multiple oxidation states, high theoretical specific capacitance, reversible small ions storage and low cost [11]. Zhou et al. prepared MoO_2 nanoparticles, and the sample shows a high specific capacitance of 621 F g^{-1} [17], and Wu et al. investigated the properties of MoO_2/CNTs with the capacitance of 467.4 F g^{-1} [18].

Mixed metal oxides have attracted much attention because of its high redox activity, good electrical conductivity, reversible small ions storage, and low cost [11]. Among them, the metal molybdates have attracted much attention for energy storage application. Such as $NiMoO_4$ [19–21], $MnMoO_4$ [22, 23], $CoMoO_4$ [6, 8, 11, 24, 25] and other metal molybdates have been extensively investigated as excellent electrode materials for supercapacitor. As reported in Refs. [26–28], $CoMoO_4$ is advantageous because of its low cost and non-toxicity and exhibits enhanced electrochemical properties. Veerasubramani et al. prepared the plate-like $CoMoO_4$ with a specific capacitance of about 133 F g^{-1} at 1 mA cm^{-2} [26]. Padmanathan et al. synthesized the α-$CoMoO_4$ nanoflakes/CFC used as symmetric supercapacitor with

* Correspondence: xwwang2000@163.com
Laboratory of Functional Materials and Henan Key Laboratory of Photovoltaic Materials, College of Physics and Materials Science, Henan Normal University, No. 46 Construction East Road, Xinxiang 453007, Henan, China

a specific capacitance of 8.3 F g^{-1} at a current density of 1 A g^{-1} in organic electrolyte [29]. In addition, Kazemi et al. obtained the dandelion-shape $CoMoO_4$ with an excellent specific capacitance of 2100 F g^{-1} at a current density of 1 A g^{-1} [8]. Xia et al. reported that the $CoMoO_4$/graphene composites show a specific capacitance of 394.5 F g^{-1} (at the scan rate of 1 mV s^{-1}), which is about 5.4 times the value of pure $CoMoO_4$ [30].

In this article, the $CoMoO_4$ nanoflakes were synthesized by a simple hydrothermal method at different hydrothermal reaction time, followed by calcining at 400 °C in muffle furnace. The electrochemical properties of samples were investigated by using the methods of cyclic voltammetry (CV), galvanostatic charge-discharge (GCD), and electrochemical impedance spectroscopy (EIS). According to GCD test results, the samples show specific capacitances of 151, 182, 243, 384, and 186 F g^{-1} at current density of 1 A g^{-1} in 2 M KOH electrolyte. The sample CMO-12 shows an interesting electrochemical property.

Experimental

Synthesis of $CoMoO_4$

The $CoMoO_4$ samples were synthesized by a simple hydrothermal method. Firstly, 0.4410 g $Co(NO_3)_2{\cdot}6H_2O$ and 0.2675 g $(NH_4)_6Mo_7O_{24}{\cdot}4H_2O$ (AHM) were dissolved in 30-mL distilled water with magnetic stirring for 10 min at room temperature to obtain clear mixed solution. Secondly, 0.3621 g urea was slowly added into the mixed solution of $Co(NO_3)_2{\cdot}6H_2O$ and AHM under magnetic stirring. The mixture was stirred for 1 h to form a homogeneous solution. Next, the homogeneous solution was transferred into a 50-mL Teflon-lined stainless steel autoclave and maintained at 180 °C in an electric oven for 1 h. Other samples were prepared with the hydrothermal times of 4, 8, 12, and 24 h, respectively. The as-synthesized products were cooled to room temperature with the oven. Then, the resulting solution was centrifuged with distilled water and ethanol. The obtained precipitate was dried at 60 °C in vacuum oven for 10 h. Finally, the dried precipitate was calcined at 400 °C in muffle furnace for 2 h to obtain the final products. The final products were marked as CMO-1, CMO-4, CMO-8, CMO-12, and CMO-24, respectively.

Material Characterization

The crystalline structures of samples were determined by X-ray diffraction (XRD; Bruker, D8 Discover) at 40 kV and 40 mA. The morphologies of samples were examined by field emission scanning electron microscopy (FE-SEM; Zeiss, SUPRA 40) and transmission electron microscopy (TEM; JEM-2100). The nitrogen adsorption-desorption isotherms of samples were obtained by using the Autosorb-iQ physico-adsorption apparatus. Then, the specific surface areas and pore size distributions of samples were obtained by the Brunauer-Emmett-Teller (BET) and Barrett-Joyner-Halenda (BJH) methods.

Preparation of the Working Electrode and Electrochemical Measurements

The working electrodes were prepared according to the method reported in literature [31]. The as-synthesized products, acetylene blacks, and polytetrafluoroethylene (PTFE) were mixed with a weight ratio of 70:20:10 to form homogeneous paste. Then, it was coated onto the cleaned nickel foam with the area of 1 cm × 1 cm. After drying in a vacuum oven at 50 °C for 6 h to remove the solvent, the nickel foam was then pressed at 10 MPa for 2 min by bead machine. The mass of the active material on the electrode was about 3~5 mg.

The electrochemical properties of samples were characterized by using a CS 350 electrochemical workstation (CorrTest, Wuhan) at room temperature. Two moles per liter of KOH solutions were used as the electrolyte solution, and a three-electrode system was used in the measurement. $CoMoO_4$, platinum, and a saturated calomel electrode (SCE) were served as the working electrode, the counter electrode, and the reference electrode, respectively. The CV curves were performed in the potential range of − 0.2 to + 0.6 V at different scan rates of 5, 10, 20, 40, 50, and 100 mV s^{-1}. GCD curves were tested at different current densities of 1, 1.5, 2, 3, 5, and 8 A g^{-1}. EIS of samples were investigated from 0.01 Hz to 100 kHz.

Results and Discussion

Structural and Morphology Characterization

As shown in Fig. 1, XRD patterns of samples are consistent with the standard pattern of $CoMoO_4$ (JCPDS No. 21-0868), and they are similar as reported in previous [6, 8,

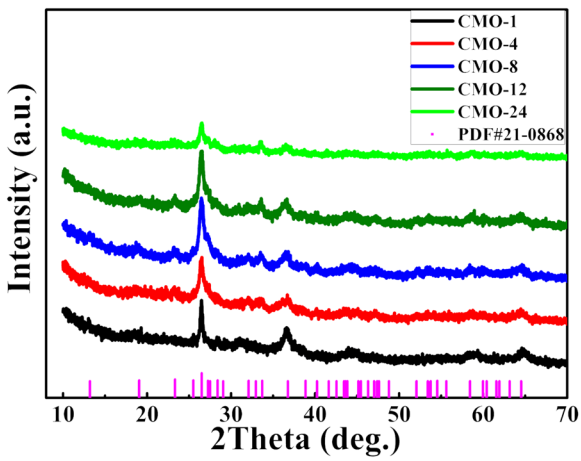

Fig. 1 XRD patterns of five samples

32, 33]. The diffraction peaks at 13.1°, 19.1°, 23.3°, 26.5°, 27.2°, 28.3°, 32.0°, 33.6°, 36.7°, 40.2°, 43.6°, 47.0°, 52.1°, 53.7°, 58.4°, and 64.5° are corresponding to reflections of the (001), ($\bar{2}$01), (021), (002), ($\bar{1}$12), ($\bar{3}$11), ($\bar{1}$31), ($\bar{2}$22), (400), (003), ($\bar{2}$41), (241), ($\bar{2}$04), ($\bar{4}$41), (024), and (243) planes, respectively. As shown in Fig. 1, the broader and weaker diffraction peaks of the XRD patterns for $CoMoO_4$ samples were observed, indicating the weaker crystallization in samples. As reported in Refs. [8, 34], the weaker crystallinity plays a critical role for enhancing the electrochemical behavior in supercapacitor applications.

The surface morphologies of $CoMoO_4$ samples were characterized by SEM and TEM. As shown in Fig. 2, microsphere structures were observed for all samples, and the microsphere consisted of nanoflakes. With the increase of hydrothermal time, the thickness of

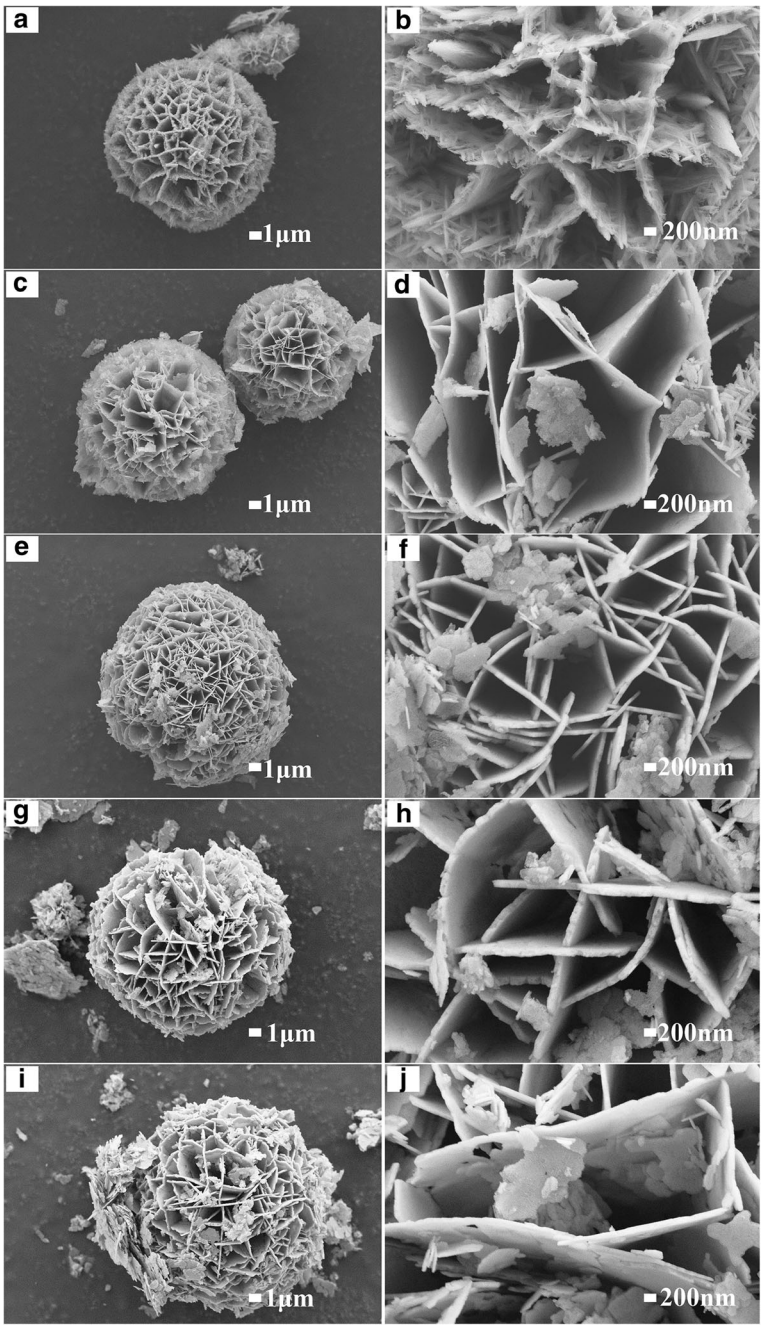

Fig. 2 The low and high-magnification SEM images of samples. **a**, **b** CMO-1. **c**, **d** CMO-4. **e**, **f** CMO-8. **g**, **h** CMO-12. **i**, **j** CMO-24

nanosheetsincreases first and then decreases, and the thickest nanoflakes were obtained in sample with the hydrothermal time of 12 h. Figure 3a, b show the energy-dispersive spectroscopy (EDS) element mapping images and EDS spectrum of CMO-12. According to the element mapping images, Co, Mo, and O elements uniformly distributed in the microsphere. The element molar ratio of Co, Mo, and O is about 1:1:4, which is corresponding to the composition of $CoMoO_4$. Figure 3c, d show the TEM images of the CMO-12. As shown in the inset of Fig. 3c, the selected area electron diffraction (SAED) patterns reveal the single-crystalline nature of the $CoMoO_4$. The clear diffraction spots could be assigned to the $(\bar{2}\,22)$, (024), $(\bar{1}\,31)$, and (002) crystal planes of the $CoMoO_4$. Figure 3d is the HRTEM image; it shows the lattice spacing of 0.34 and 0.27 nm, which could be related to the (002) and $(\bar{1}31)$ planes of $CoMoO_4$, respectively.

Figure 4 shows the pore size distributions and N_2 adsorption-desorption isotherms of $CoMoO_4$ samples. According to the N_2 adsorption-desorption isotherms of samples, all the isotherms show the feature of type IV with H_3-type hysteresis loops. The BET specific surface areas of CMO-1, CMO-4, CMO-8, CMO-12, and CMO-24 were calculated to be 18.4, 29.2, 42.8, 74.1, and 26.2 $m^2\ g^{-1}$, respectively. Sample CMO-12 shows the highest BET surface area, and the high BET surface area could increase the contact area of electrode/electrolyte and provide more active sites for efficient transport of electrons and ions in electrode system [35]. As shown in Fig. 4, sharp peaks in pore size distributions of samples are located at 145.9, 74.1, 22.6, 27.9, and 75.3 nm, respectively. It indicates that there are mesopores in CMO-8 and CMO-24. However, a few macropores are detected in samples CMO-1, CMO-4, and CMO-24. When materials are used in supercapacitors, mesopore structures of materials also could increase the contact area between electrode and electrolyte; there are more sufficient active sites for efficient transport of electrons and ions in electrode system [36–38]. Therefore, CMO-12 with highest BET surface area and mesopore structure might show better electrochemical properties than other samples.

Electrochemical Characterization

CV curves of $CoMoO_4$ samples at different scan rates of 5–100 mV s^{-1} in 2 M KOH electrolyte with potential range from − 0.2 V to + 0.6 V (vs. Hg/HgO) are shown in Fig. 5a –e. The typical Faradic reaction peaks can be clearly seen in all curves, which indicate that the $CoMoO_4$ electrodes are pseudocapacitor electrodes. The observed redox peak is due to the charge-transfer kinetics of Co^{2+} and Co^{3+} associated with the OH^- in electrolyte

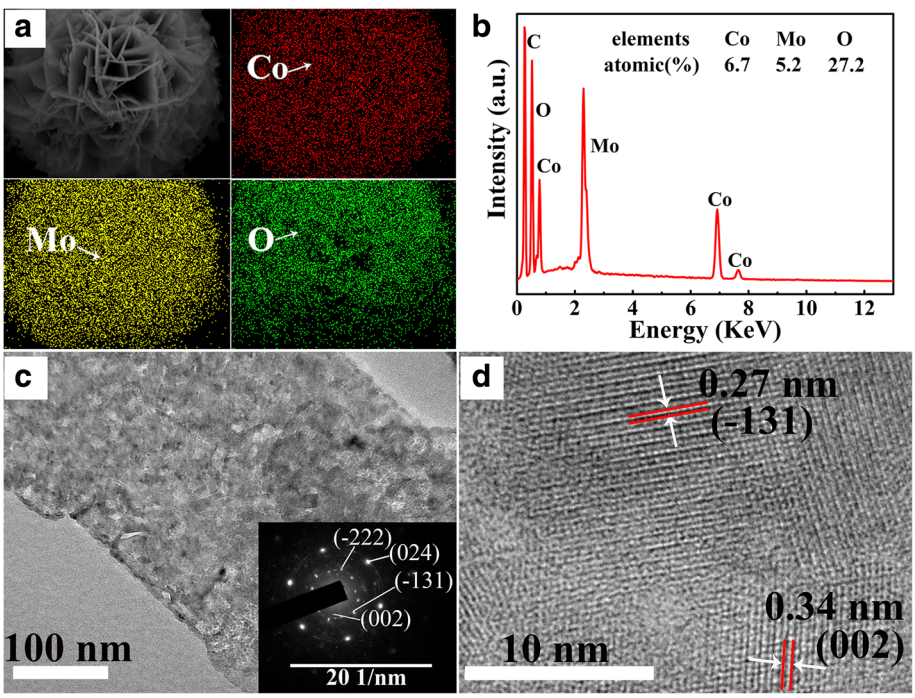

Fig. 3 **a** Energy-dispersive spectroscopy (EDS) element mapping image and Co, Mo, and O distribution. **b** The EDS spectrum and inset are molar ration percent of Co, Mo, and O elements. **c** High-magnification TEM and inset are the selected area electron diffraction pattern. **d** The HRTEM image of CMO-12 sample

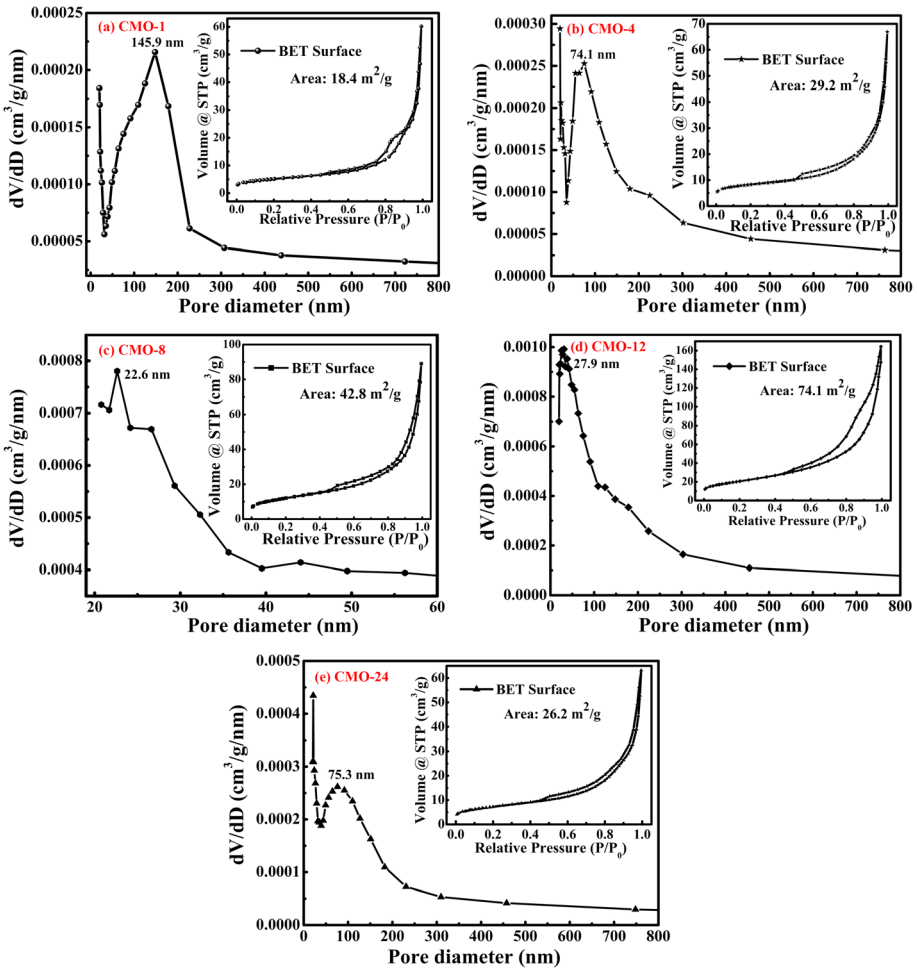

Fig. 4 Pore size distributions and N_2 adsorption-desorption isotherms of samples

[8, 26]. The redox reaction of Co^{2+}/Co^{3+} is listed as follows [39, 40]:

$$CoMoO_4 + OH^- \rightarrow CoOOH + MoO_3 + e^- \quad (1)$$

$$CoOOH + OH^- \Leftrightarrow CoO_2 + H_2O + e^- \quad (2)$$

$$CoOOH + H_2O + e^- \Leftrightarrow Co(OH)_2 + OH^- \quad (3)$$

As shown in Fig. 5a–e, with the increase of scan rates, the redox peaks shift to higher and lower potentials, respectively. The potential difference between oxidation peaks and reduction peaks also increased with the increased scan rate. It indicates that the irreversible degree and the quasi-reversible reaction are increased with the increase of scan rate [36, 41]. The shift is mainly related to the internal resistance of the electrode and the polarization caused by high scan rate [36, 42]. A near linearly relationship between redox peaks potentials and the square root of the scan rate was observed, which can be seen in the inset of Fig. 5f. The approximately linear relationship also indicates that the reaction kinetics during redox process is probably controlled by ions diffusion process [6].

According to the CV curves, the specific capacitance of samples can be calculated by the following equation:

$$C_{sp} = \frac{\int_{V_1}^{V_2} IdV}{m \times v \times \Delta V}, \quad (4)$$

where C_{sp} (F g^{-1}) is the specific capacitance, V_1 and V_2 are the start and end voltage, $\int IdV$ is the integral area of CV curves, m (g) is the mass of active materials loading on the electrode, v (mV s^{-1}) is the potential scan rates, and ΔV (V) is the sweep potential window. The specific capacitances of samples were calculated based on the CV curves by using Eq. (4), which are shown in Fig. 5f. The specific capacitances of all samples decrease as the increase of scan rates. More OH^- can reach the active site with more favorable conditions at low potential scan

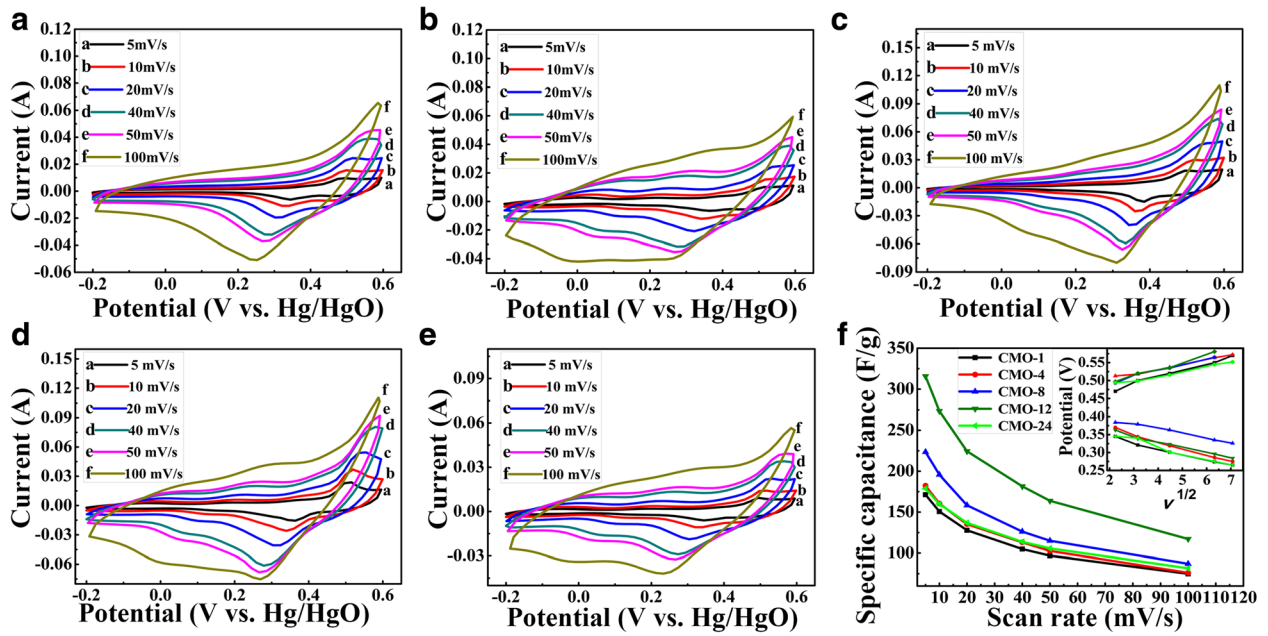

Fig. 5 The CV curves under different scan rates of 5, 10, 20, 40, 50, and 100 mV s^{-1} of samples **a** CMO-1, **b** CMO-4, **c** CMO-8, **d** CMO-12, and **e** CMO-24 in the potential window ranged from − 0.2 to + 0.6 V. **f** The specific capacitance of samples under different scan rates of 5–100 mV s^{-1}. The inset in **f** is the plots of anodic and cathodic peak current against the square root of the scan rate

rate [31, 43]. Furthermore, a higher scan rate leads to either depletion or saturation of the protons in the electrolyte inside the electrode during the redox process, and only the outer surface could be utilized for the charge storage [41, 43, 44]. When the hydrothermal synthesis time increases from 1 to 12 h, the specific capacitances of samples show an obviously increase from 171.3 to 315.7 F g^{-1} at a scan rate of 5 mV s^{-1}. However, the specific capacitance decreases from 315.7 to 178.7 F g^{-1} when the hydrothermal time increases from 12 to 24 h. Therefore, the CMO-12 sample (i.e., the hydrothermal time is 12 h) shows an excellent specific capacitance. The specific capacitance of 315.7 F g^{-1} at 5 mV s^{-1} is better than that of 286 F g^{-1} for $CoMoO_4$ nanorods [11] and 95.0 F g^{-1} for pure $CoMoO_4$ [45] and comparable with 322.5 F g^{-1} for RGO/$CoMoO_4$ [45].

Such an improved electrochemical property can be confirmed by the following galvanostatic charge-discharge tests. The GCD tests of samples were performed at different current densities of 1, 1.5, 2, 3, 5, and 8 A g^{-1} in 2 M KOH electrolyte, and the results are shown in Fig. 6a–e. The nonlinear GCD curves could be attributed by the redox reaction [46], and this is consistent with the CV curves. As shown in these curves, the discharge time of CMO-12 is significantly longer than other samples, indicating a much higher specific capacitance in CMO-12. This could be confirmed furtherly by the following calculated results. The specific capacitances of $CoMoO_4$ electrode can be calculated by using the equation as follow:

$$C = \frac{I \times \Delta t}{m \times \Delta V}, \tag{5}$$

where C (F g^{-1}) is the specific capacitance, I (A) is the discharge current, Δt (s) is refer to discharge times, m (g) is the mass of active material loading on the electrode surface, and ΔV (V) is the applied potential window [6, 8, 26]. Figure 6f shows the calculated specific capacitance of samples at different current densities. With the increase of current density, the specific capacitances of samples are decreased. This can be attributed to the effective contact between ions and electro-active sites of electrode. At high current density, there is only part of the total available reaction sites because the electrolyte ions suffer from low diffusion, which lead to an incomplete insertion reaction and a low specific capacitance [19, 45]. From Fig. 6f, we can see that the CMO-12 has the highest specific capacitance, which are 384, 337, 307, 269, 229, and 172 F g^{-1} at the current density of 1, 1.5, 2, 3, 5, and 8 A g^{-1}, respectively. The specific capacitance of CMO-12 shows a good rate capability. Furthermore, the specific capacitance of CMO-12 is also higher than that reported in some previous literatures. As reported by Tian et al. [39], the specific capacitance of needle-like Co-Mo-O is 302 F g^{-1} at a current density of 1 A g^{-1}. The maximum

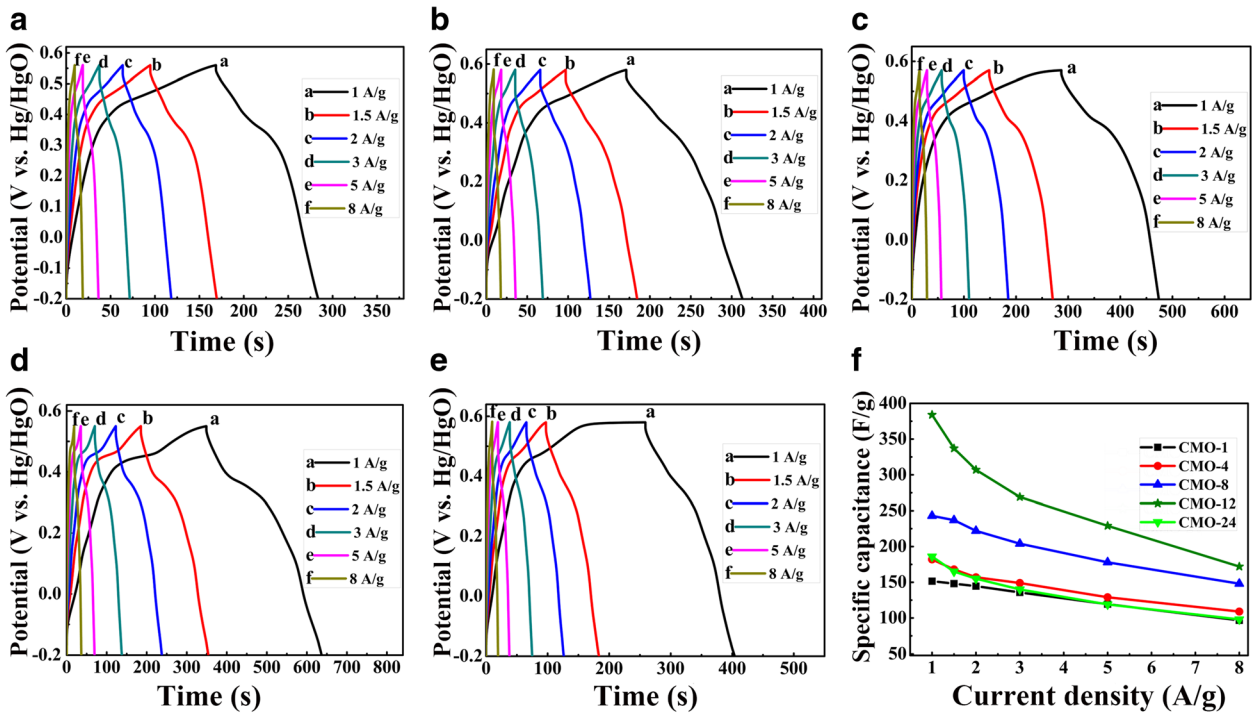

Fig. 6 The GCD curves under different current densities of 1, 1.5, 2, 3, 5, and 8 A g^{-1} of samples **a** CMO-1, **b** CMO-4, **c** CMO-8, **d** CMO-12, and **e** CMO-24 in the potential window ranged from − 0.2 to + 0.58 V. **f** The specific capacitance of samples calculated by GCD results

specific capacitance of $CoMoO_4$ was about 133 F g^{-1} at 1 mA cm^{-2} in the article of Veerasubramani [26]. In Ref. [29], the specific capacitance of α-$CoMoO_4$ nanoflakes/CFC used as symmetric supercapacitor is only 8.3 F g^{-1} at current density of 1 A g^{-1}. Besides, a high discharge rate or a high current density is very important for a real supercapacitor device, which involves a fast charging-discharging process [43]. At a high current density of 8 A g^{-1}, the specific capacitances for the five samples are 97, 109, 148, 172, and 98 F g^{-1}, respectively.

The stabilities of the $CoMoO_4$ electrodes were detected in 2 M KOH electrolyte at a current density of 8 A g^{-1} for 1000 cycles, which are shown in Fig. 7. After 1000 cycles, the five samples show the retention of 102.9, 87.8, 101.5, 94.2, and 100.5%, respectively. For the increase of specific capacitance during the cyclic charge-discharge process, it could be ascribed to activation of the $CoMoO_4$ surface with time [6]. It makes the surface of $CoMoO_4$ contact fully with the electrolyte, which leads to the improvement of electrochemical property [6, 47, 48]. Figure 7b shows the coulombic efficiency of $CoMoO_4$ samples during the 1000 charge-discharge cycles, which also shows high specific capacitance. The results indicate that all these samples have fine long-cycle stability. The highly specific capacitance, great rate capacity, and fine long-cycle stability indicate that the CMO-12 sample has an excellent electrochemical property.

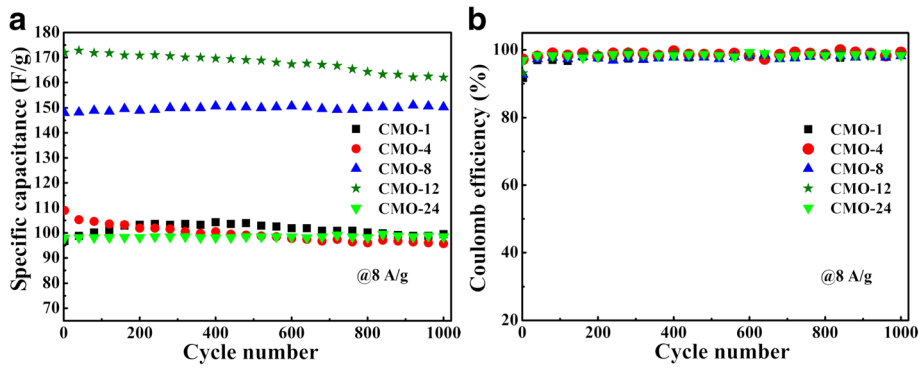

Fig. 7 a Cycling performance of the electrodes at 8 A g^{-1}. **b** The corresponding coulombic efficiency of samples during cycling test

To further evaluate the electrochemical property of $CoMoO_4$ electrode, the EIS of five samples are recorded in 2 M KOH electrolyte. Figure 8 is the Nyquist plots of five samples. The Nyquist plots represent the frequency response of the electrode/electrolyte system [26, 49]. The EIS spectra can be fitted by the equivalent circuit diagram, which was inserted in Fig. 8. The Nyquist plot is composed of a semicircle at high frequency and a straight line at low frequency. The semicircle diameter at high frequency represents the Faraday interface charge transfer resistance (R_{ct}), and the slope of the straight line at low frequency is the representative of the typical Warburg resistance (W_0) [41], respectively. CPE1 is a constant phase element, accounting for the double-layer capacitance [43]. In addition, the series resistance R_s is the internal resistance, which could be obtained from the intercept of the plots on the real axis [11]. The measured R_s values are 2.83, 2.41, 1.51, 1.22, and 2.26 Ω for the five samples, respectively. And the fitted R_{ct} values of the five samples are1.69, 1.48, 0.72, 0.23, and 1.28 Ω. The EIS results show that the CMO-12 sample has lower values of R_s and R_{ct} than the other four samples. This indicates that the CMO-12 sample has higher electronic and ionic conductivities than the other samples [35, 50, 51]. Besides, CMO-12 with mesopores structure has higher BET surface area than the other samples. The high BET surface area and good conductivity are benefic for redox reaction in electrode/electrolyte system.

Conclusions

In summary, the $CoMoO_4$ microspheres have been successfully synthesized by hydrothermal growth process coupled with calcinations treatment. The hydrothermal synthesis times are 1, 4, 8, 12, and 24 h, respectively. XRD patterns indicate that single phase $CoMoO_4$ structure was obtained. SEM images show the microspheres were composed of nanoflakes. The CMO-12, which was prepared with the hydrothermal time of 12 h, has demonstrated an excellent supercapacitor performance. According to GCD tests, the specific capacitances of CMO-12 are 384, 337, 307, 269, 229, and 172 F g^{-1} at current densities of 1, 1.5, 2, 3, 5, and 8 A g^{-1}, respectively, while it just reached 151, 182, 243, or 186 F g^{-1} at the current density 1 A g^{-1} for other samples with different hydrothermal times. The retain capacitances of CMO-12 sample after 1000 charging-discharging cycles at current density of 8 A g^{-1} show the fine long-cycle stability. Such excellent capacitive behavior could be ascribed to the microsphere structure and high BET surface area, and the good conductivity in CMO-12 electrode is also helpful to the improvement of capacitive behavior. The high specific capacitance, good rate capability, and excellent cycling stability promote the practical application of $CoMoO_4$ materials in supercapacitors.

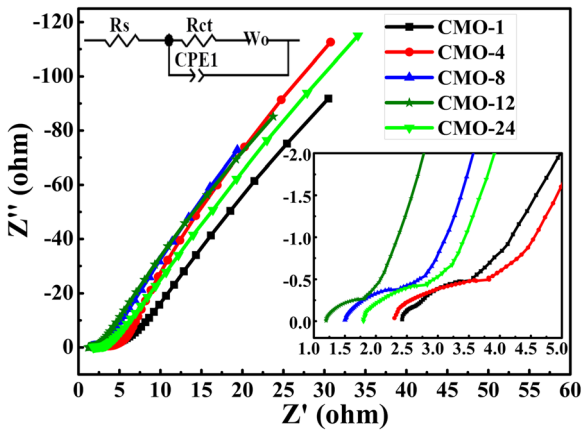

Fig. 8 EIS spectrums of samples obtained at the frequency ranging from 0.01 Hz to 100 KHz. The inset is the local amplification of EIS spectrums and the equivalent circuit diagram

Abbreviations

BET: Brunauer-Emmett-Teller; CV: Cyclic voltammetry; EDS: Energy-dispersive spectroscopy; EIS: Electrochemical impedance spectroscopy; FE-SEM: Field emission scanning electron microscopy; GCD: Galvanostatic charge-discharge; PTFE: Polytetrafluoroethylene; SAED: Selected area electron diffraction; SCE: Saturated calomel electrode; TEM: Transmission electron microscopy; XRD: X-ray diffraction

Funding

This work has been supported by the National Natural Science Foundation of China (No. 51402091, No. 51601059, No. 11304082, and No. 11404102), the scientific research foundation for new introduced doctors in Henan Normal University (No. 11114), and the National University Student Innovation Program (No. 201410476037).

Availability of Data and Materials

All data and materials are available.

Authors' Contributions

WXL, XWW, and YCH conceived the project. WXL, LYS, and CG carried out the experiment and data analysis and finalized the manuscript. CCZ, HL, and MD provided helpful proposal for the experiment. All authors read and approved the final manuscript.

Competing Interests

The authors declare that they have no competing interests.

Publisher's Note

Received: 3 January 2018 Accepted: 17 April 2018
Published online: 24 April 2018

References

1. Watcharatharapong T, Sundaram MM, Chakraborty S, Li D, Shafiullah GM, Aughterson RD, Ahuja R (2017) Effect of transition metal cations on stability enhancement for molybdate-based hybrid supercapacitor. ACS Appl Mater Inter 9:17977–17991
2. Cho J, Jeong S, Kim Y (2015) Commercial and research battery technologies for electrical energy storage applications. Prog Energ Combust 48:84–101
3. Bao L, Li T, Chen S, Peng C, Li L, Xu Q, Chen YS, Ou E, Xu WJ (2017) 3D graphene frameworks/Co_3O_4 composites electrode for high-performance supercapacitor and enzymeless glucose detection. Small 13:1602077
4. Wang XW, Wang XE, Zhang HC, Zhu QQ, Zheng DL, Sun LY (2017) Preparation and electrochemical properties of $LaMnO_3$ powder as a supercapacitor electrode material. Key Eng Mater 727:698–704

5. Dhankhar S, Menon SS, Gupta B, Baskar K, Singh S (2017) Electrochemical performance of brownmillerite calcium ferrite for application as supercapacitor. AIP Conf Proc 1832:080050
6. Candler J, Elmore T, Gupta BK, Dong L, Palchoudhury S, Gupta RK (2015) New insight into high-temperature driven morphology reliant $CoMoO_4$ flexible supercapacitor. New J Chem 39:6108–6116
7. Zhang ZY, Xiao F, Xiao J, Wang S (2015) Functionalized carbonaceous fibers for high performance flexible all-solid-state asymmetric supercapacitors. J Mater Chem A 3:11817–11823
8. Kazemi SH, Tabibpour M, Kiani MA, Kazemi H (2016) An advanced asymmetric supercapacitor based on a binder-free electrode fabricated from ultrathin $CoMoO_4$ nano-dandelions. RSC Adv 6:71156–71164
9. Li M, Wang YH, Yang HX, Chu PK (2017) Hierarchical $CoMoO_4$@Co_3O_4 nanocomposites on an ordered macro-porous electrode plate as a multi-dimensional electrode in high-performance supercapacitors. J Mater Chem A 5:17312–17324
10. Li WY, He GJ, Shao JJ, Liu Q, Xu KB, Hu JQ, Parkin IP (2015) Urchin-like MnO_2 capped ZnO nanorods as high-rate and high-stability pseudocapacitor electrodes. Electrochim Acta 186:1–6
11. Liu MC, Kong LB, Lu C, Li XM, Luo YC, Kang L (2013) Facile fabrication of $CoMoO_4$ nanorods as electrode material for electrochemical capacitors. Mater Lett 94:197–200
12. Vijayakumar S, Nagamuthu S, Muralidharan G (2013) Supercapacitor studies on NiO nanoflakes synthesized through a microwave route. ACS Appl Mater Inter 5:2188–2196
13. Yan H, Zhang D, Xu J, Lu Y, Liu Y, Qiu K, Zhang Y, Luo Y (2014) Solution growth of NiO nanosheets supported on Ni foam as high-performance electrodes for supercapacitors. Nanoscale Res Lett 9:424
14. Bhise SC, Awale DV, Vadiyar MM, Patil SK, Kokare BN, Kolekar SS (2017) Facile synthesis of CuO nanosheets as electrode for supercapacitor with long cyclic stability in novel methyl imidazole-based ionic liquid electrolyte. J Solid State Electr 21:2585–2591
15. Liu T, Jiang CJ, You W, Yu JG (2017) Hierarchical porous C/MnO_2 composite hollow microspheres with enhanced supercapacitor performance. J Mater Chem A 5:8635–8643
16. Xiao HH, Yao SY, Qu FY, Zhang X, Wu X (2017) Electrochemical energy storage performance of heterostructured SnO_2@MnO_2 nanoflakes. Ceram Int 43:1688–1694
17. Zhou E, Wang CG, Zhao QQ, Li ZP, Shao MH, Deng XL, Liu XJ, Xu XJ (2016) Facile synthesis of MoO_2 nanoparticles as high performance supercapacitor electrodes and photocatalysts. Ceram Int 42:2198–2203
18. Wu JZ, Li XY, Zhu YR, Yi TF, Zhang JH, Xie Y (2016) Facile synthesis of MoO_2 /CNTs composites for high-performance supercapacitor electrodes. Ceram Int 42:9250–9256
19. Ghosh D, Giri S, Das CK (2013) Synthesis, characterization and electrochemical performance of graphene decorated with 1D $NiMoO_4 \cdot nH_2O$ nanorods. Nano 5:10428–10437
20. Ezeigwe ER, Khiew PS, Siong CW, Kong I, Tan MTT (2017) Synthesis of $NiMoO_4$ nanorods on graphene and superior electrochemical performance of the resulting ternary based composites. Ceram Int 43:13772–13780
21. Yan Z, Jie X, Zheng YY, Zhang YJ, Xing H, Xu TT (2017) $NiCo_2S_4$@$NiMoO_4$ core-shell heterostructure nanotube arrays grown on Ni foam as a binder-free electrode displayed high electrochemical performance with high capacity. Nanoscale Res Lett 12:412
22. Johnbosco Y, Elumalai V, Bhagavathiachari M, Samuel AS, Elaiyappillai E, Johnson PM (2017) A facile sonochemical assisted synthesis of α-$MnMoO_4$/PANI nanocomposite electrode for supercapacitor applications. J Electroanal Chem 797:78–88
23. Wang H, Song YH, Zhou JK, Xu XY, Hong W, Yan J, Xue RN, Zhao HL, Liu Y, Gao JP (2016) High-performance supercapacitor materials based on polypyrrole composites embedded with core-sheath polypyrrole@$MnMoO_4$ nanorods. Electrochim Acta 212:775–783
24. Guo D, Zhang HM, Yu XZ, Zhang M, Zhang P, Li QH, Wang TH (2013) Facile synthesis and excellent electrochemical properties of $CoMoO_4$ nanoplate arrays as supercapacitors. J Mater Chem A 1:7247–7254
25. Hu JY, Qian F, Song GS, Wang LL (2016) Hierarchical heterostructures of $NiCo_2O_4$@$XMoO_4$ (X = Ni, co) as an electrode material for high-performance supercapacitors. Nanoscale Res Lett 11:257
26. Veerasubramani GK, Krishnamoorthy K, Radhakrishnan S, Kim NJ, Sang JK (2014) Synthesis, characterization, and electrochemical properties of $CoMoO_4$ nanostructures. Int J Hydrogen Energ 39:5186–5193
27. Senthilkumar B, Meyrick D, Lee Y-S, Selvan RK (2013) Synthesis and improved electrochemical performances of nano β-$NiMoO_4$-$CoMoO_4 \cdot xH_2O$ composites for asymmetric supercapacitors. RSC Adv 3:16542–16548
28. Ding Y, Wan Y, Min YL, Zhang W, Yu SH (2008) General synthesis and phase control of metal molybdate hydrates $MMoO_4.nH_2O$ (M = Co, Ni, Mn, n = 0, 3/4, 1) nano/microcrystals by a hydrothermal approach: magnetic, photocatalytic, and electrochemical properties. Inorg Chem 47:7813–7823
29. Padmanathan N, Han S, Selladurai S, Glynn C, O'Dwyer C, Razeeb KM (2015) Pseudocapacitance of α-$CoMoO_4$ nanoflakes in non-aqueous electrolyte and its bi-functional electro catalytic activity for methanol oxidation. Int J Hydrogen Energ 40:16297–16305
30. Xia XF, Wu L, Hao QL, Wang WJ, Wang X (2013) One-step synthesis of $CoMoO_4$/graphene composites with enhanced electrochemical properties for supercapacitors. Electrochim Acta 99:253–261
31. Wang XW, Zheng DL, Yang PZ, Wang XE, Zhu QQ, Ma PF, Sun LY (2016) Preparation and electrochemical properties of NiO-Co_3O_4 composite as electrode materials for supercapacitors. Chem Phys Lett 667:260–266
32. Rico JL, Ávalos-Borja M, Barrera A, Hargreaves JSJ (2013) Template-free synthesis of $CoMoO_4$ rods and their characterization. Mater Res Bull 48:4614–4617
33. Li M, Xu SH, Cherry C, Zhu YP, Wu DJ, Zhang C, Zhang XL, Huang R, Qi RJ, Wang LW (2015) Hierarchical 3-dimensional $CoMoO_4$ nanoflakes on a macroporous electrically conductive network with superior electrochemical performance. J Mater Chem A 3:13776–13785
34. Liu MC, Kong LB, Kang L, Li XH, Walsh FC, Xing M, Lu C, Ma XJ, Luo YC (2014) Synthesis and characterization of $M_3V_2O_8$ (M = Ni or Co) based nanostructures: a new family of high performance pseudocapacitive materials. J Mater Chem A 2:4919–4926
35. Zhao Y, Liu Z, Gu W, Zhai Y, Teng Y, Teng F (2016) Enhanced energy density of a supercapacitor using 2D $CoMoO_4$ ultrathin nanosheets and asymmetric configuration. Nanotechnology 27:505401
36. Wang XW, Li WX, Wang XE, Zhang JJ, Sun LY, Gao C, Shang J, Hu YC, Zhu QQ (2017) Electrochemical properties of $NiCoO_2$ synthesized by hydrothermal method. RSC Adv 7:50753–50759
37. Lei Y, Li J, Wang Y, Gu L, Chang Y, Yuan H, Xiao D (2014) Rapid microwave-assisted green synthesis of 3D hierarchical flower-shaped $NiCo_2O_4$ microsphere for high-performance supercapacitor. ACS Appl Mater Interfaces 6:1773–1780
38. Liu X, Zhao J, Cao Y, Li W, Sun Y, Lu J, Men Y, Hu J (2015) Facile synthesis of 3D flower-like porous NiO architectures with an excellent capacitance performance. RSC Adv 5:47506–47510
39. Tian YP, Zhou M, Meng XR, Miao YQ, Zhang DW (2017) Needle-like Co-Mo-O with multi-modal porosity for pseudocapacitors. Mater Chem Phys 198:258–265
40. Chen Y, Kang GY, Xu H, Kang L (2016) Two composites based on $CoMoO_4$ nanorods and PPy nanoparticles: fabrication, structure and electrochemical properties. Synthetic Met 215:50–55
41. Wang XW, Zhu QQ, Wang XE, Zhang HC, Zhang JJ, Wang LF (2016) Structural and electrochemical properties of $La_{0.85}Sr_{0.15}MnO_3$ powder as an electrode material for supercapacitor. J Alloy Compd 675:195–200
42. Zhang GQ, Lou XW (2013) General solution growth of mesoporous $NiCo_2O_4$ nanosheets on various conductive substrates as high-performance electrodes for supercapacitors. Adv Mater 25:976–979
43. Wang KB, Zhang ZY, Shi XB, Wang HJ, Lu YN, Ma XY (2015) Temperature-dependent self-assembly of NiO/Co_3O_4 composites for supercapacitor electrodes with good cycling performance: from nanoparticles to nanorod arrays. RSC Adv 5:1943–1948
44. Rakhi RB, Chen W, Cha D, Alshareef HN (2012) Substrate dependent self-organization of mesoporous cobalt oxide nanowires with remarkable pseudocapacitance. Nano Lett 12:2559–2567
45. Xu XW, Shen JF, Li N, Ye MX (2014) Microwave-assisted synthesis of graphene/$CoMoO_4$ nanocomposites with enhanced supercapacitor performance. J Alloy Compd 616:58–65
46. Zhao YX, Teng F, Liu ZL, Du Q, Xu JJ, Teng YR (2016) Electrochemical performances of asymmetric supercapacitor fabricated by one-dimensional $CoMoO_4$ nanostructure. Chem Phys Lett 664:23–28
47. Liu MC, Kong LB, Ma XJ, Lu C, Li XM, Luo YC, Kang L (2012) Hydrothermal process for the fabrication of $CoMoO_4 \cdot 0.9H_2O$ nanorods with excellent electrochemical behavior. New J Chem 36:1713–1716
48. Tang W, Tian S, Liu LL, Li L, Zhang HP, Yue YB, Bai Y, Wu YP, Zhu K (2011) Nanochain $LiMn_2O_4$ as ultra-fast cathode material for aqueous rechargeable lithium batteries. Electrochem Commun 13:205–208

49. Senthilkumar ST, Selvan RK, Ponpandian N, Melo JS (2012) Redox additive aqueous polymer gel electrolyte for an electric double layer capacitor. RSC Adv 2:8937–8940
50. Lv B, Li P, Liu Y, Lin S, Gao B, Lin B (2018) Nitrogen and phosphorus co-doped carbon hollow spheres derived from polypyrrole for high-performance supercapacitor electrodes. Appl Surf Sci 437:169–175
51. Mirzaee M, Dehghanian C, Sabet BK (2018) ERGO grown on Ni-Cu foam frameworks by constant potential method as high performance electrodes for supercapacitors. Appl Surf Sci 436:1050–1060